Electronic supplementary information:

Inkjet printed paper based Frequency Selective Surfaces and skin mounted RFID tags: The interrelation between silver nanoparticle ink, paper substrate and low temperature sintering technique

Veronica Sanchez-Romaguera,[a] Sebastian Wünscher,[b] Badredin M. Turki,[c] Robert Abbel,[d] Silvia Barbosa,[e] Daniel J. Tate,[a] Dumtoochukwu Oyeka,[c] John C. Batchelor,[c] Edward A. Parker,[c] Ulrich S. Schubert,[b] and Stephen G. Yeates*[a]*

[a] Organic Materials Innovation Centre (OMIC), School of Chemistry, The University of Manchester, M13 9PL, Manchester, United Kingdom.

E-mail: veronica.sanchezromaguera@mbs.ac.uk; stephen.yeates@manchester.ac.uk

[b] Laboratory of Organic and Macromolecular Chemistry (IOMC), Friedrich Schiller University Jena, Humboldtstr. 10, 07743 Jena, Germany, and Jena Center for Soft Matter (JCSM), Friedrich Schiller University Jena, Philosophenweg 7, 07743 Jena, Germany.

[c] School of Engineering and Digital Art, University of Kent, CT2 7NT, Kent, United Kingdom.

[d] Holst Centre-TNO, High Tech Campus 31, 5656 AE Eindhoven, The Netherlands.

[e] Condensed Matter Physics Department, Faculty of Physics, Universidade de Santiago de Compostela, 15782 Santiago de Compostela, Spain.

Keywords: inkjet, FSS, RFID, paper, sintering

Substrate Characterization

The chemical nature of the PEL ink-receiving layer is not disclosed by the manufacturer. According to literature, the most common non-organic coatings for paper substrates include silica, alumina and calcium carbonate.[1,2] This type of coatings, so-called micro porous coatings, are specifically designed to concentrate the ink solute on the top surface while the solvent and dispersion agents are absorbed into the bulk of the paper, hence providing a very fast drying and fixing of the ink which results in high resolution features.[3] The characterization of PEL paper is shown in Figure S1d-f.

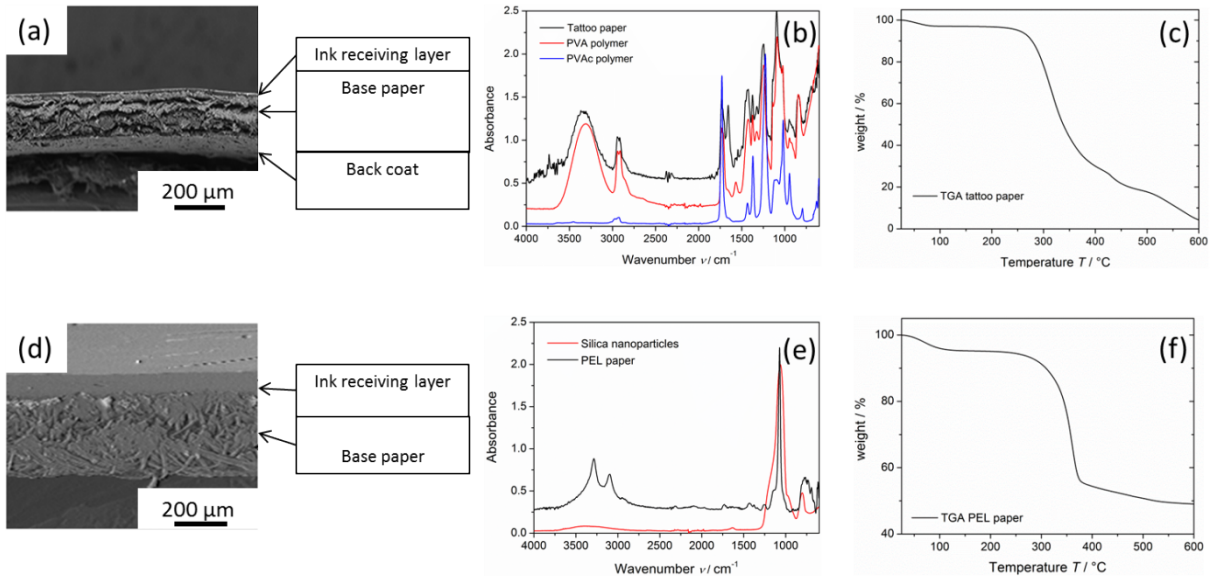

Figure S1 Cross-sectional SEM (a), FT-IR (b) and TGA (c) of tattoo paper.[4] Cross-sectional SEM (d), FT-IR (e) and TGA (f) of PEL paper. Parts reprinted with permission from The Royal Society of Chemistry.[4]

The SEM image of the cross-section of the PEL paper, Figure S1d, clearly shows two layers: A top ink-receiving layer of approximately 20 µm thickness which is attributed to the non-organic coating and a bottom paper based layer. SEM images of the surface of PEL paper reveal a top rough layer of closely packed nanoparticles, ESI Figure 3.

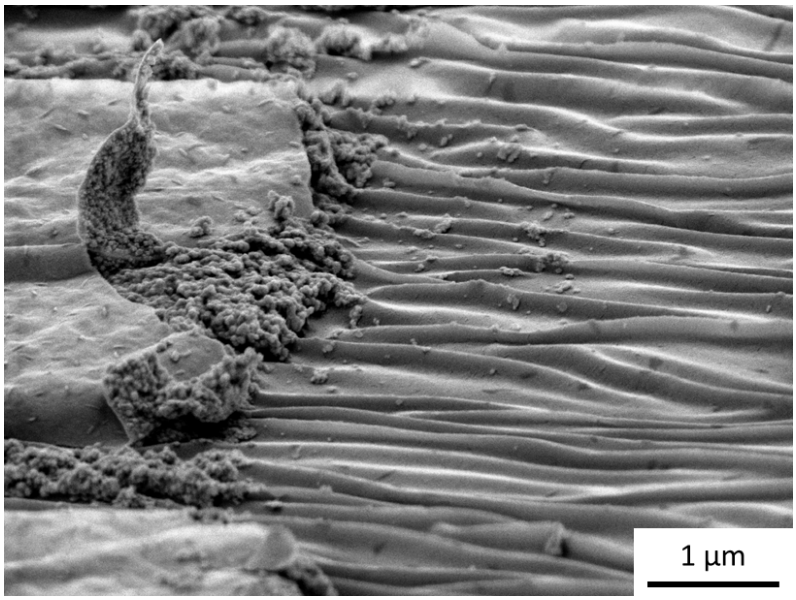

ESI Figure S2 SEM image of wrinkled surface of tattoo paper (ink receiving layer) as cause of the damage to the printed ink pattern after thermal sintering.

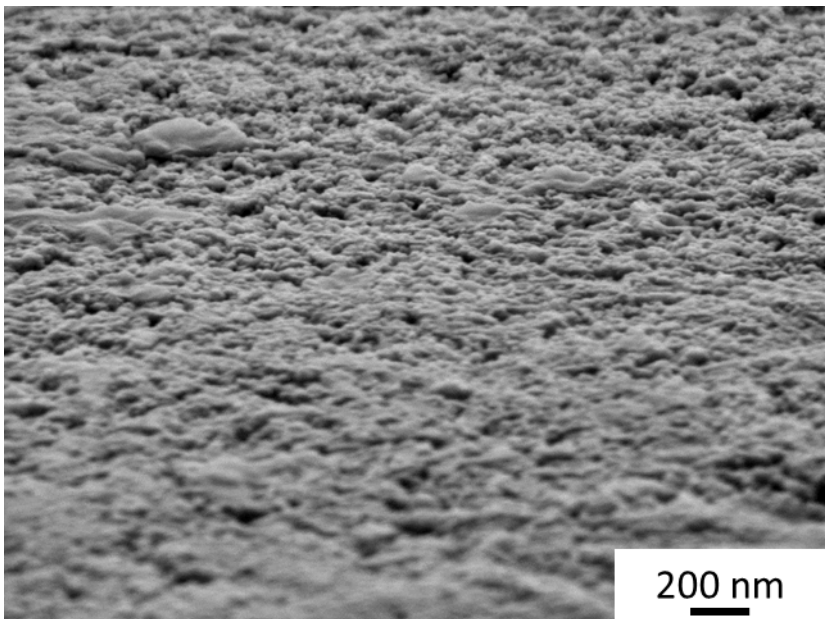

Figure S3 SEM image of the surface of PEL Nano P60 paper.

Figure S1e shows the FT-IR spectrum of the surface of PEL paper. This is compared to the FTIR spectrum of silica particles with a distinctive Si-O peak at 1,150 cm^{-1}. There is a clear match between both spectra which strongly suggests that the main component of the top layer is silica based. TGA of PEL paper, Figure S1f shows an initial mass loss of approximately 3 wt% at 100 °C, which is attributed to the loss of adsorbed moisture similar to tattoo paper

(Figure S1c) followed by a further mass loss of 42 wt% observed at approximately 365 °C which is attributed to the decomposition of the organics within the base paper layer. Compared to tattoo paper with a thinner ink-receiving layer (1 µm as displayed in Figure S1a), primarily composed of the low glass transition temperature polyvinyl alcohol (PVA) (Figure S1c) the ink receiving layer of PEL paper is considerably thicker and non-organic in nature. Hence, it is expected to be less sensitive towards temperature. According to the manufacturer, PEL paper can withstand temperatures of up to 150 °C with no coloration and higher temperatures for short periods of time.[5]

Sintering SEM Images

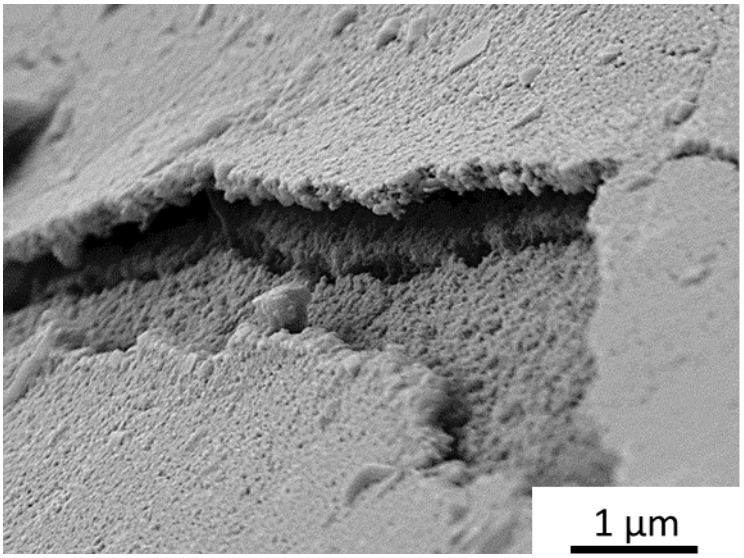

Figure S4 Cross-sectional SEM image of a photonically sintered film of Ink A on PEL paper showing a crack in the silver film but also in the silica ink-receiving layer.

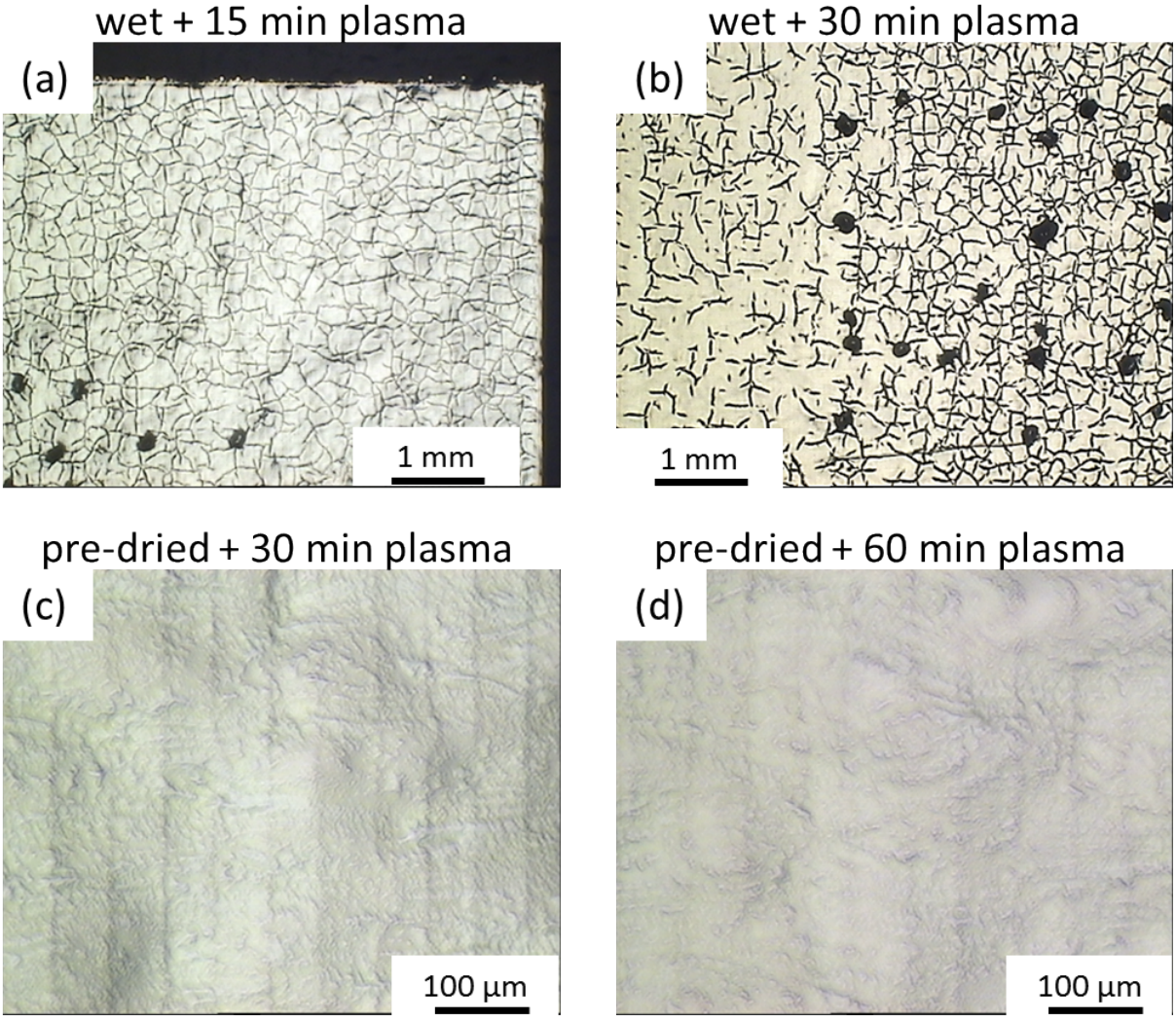

Figure S5 Microscopy images of plasma sintered patterns of: Ink A on tattoo paper after 15 min (a) and 30 min (b) without any additional pre-treatment, pre-dried (70 °C, 15 min) Ink A patterns on tattoo paper after 30 min (c) and 60 min (d).

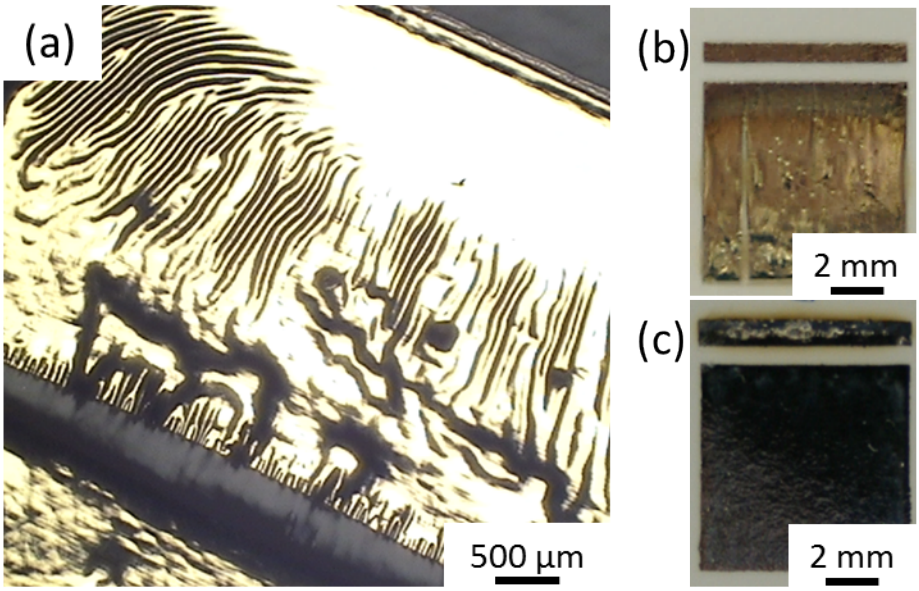

Figure S6 Microscopy image of Ink A (a) and Ink B (b,c) on tattoo paper after IPL sintering.

Device Architecture

Frequency Selective surface (FSS) design used in this work has been described in our earlier work[6] consisting of 374 patch dipoles set on a skewed lattice. The dipoles are 9.4 mm in length l with horizontal spacing D_x = 1 mm and vertical spacing D_y = 2 mm (Figure S7).

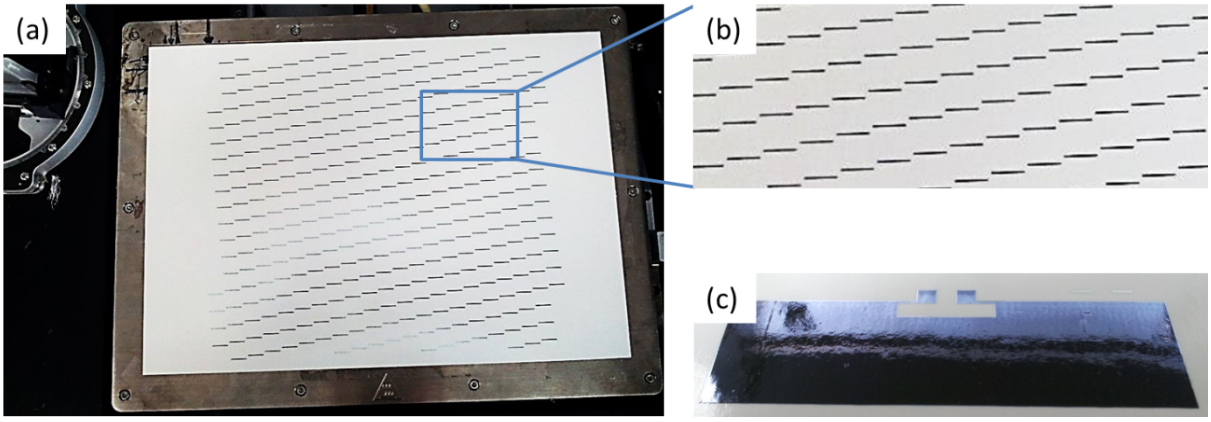

Figure S7 Inkjet printed A4 FSS array on paper situated on printer platen (a,b). Inkjet printed triple layer UHF RFID antenna with Ink A on tattoo paper (c).

All dipoles have a width of w = 0.4 mm. The physical size of the FSS is 222 × 194 mm^2. The printed FSS was mounted in a 230 × 230 mm^2 aperture cut into a large absorbing screen and

was characterized by the forward transmission scattering parameter, S_{21}, over a frequency sweep between 8 and 18 GHz. The microwave transmitter and receiver were connected to waveguide horn antennas placed 1 m in front and behind the FSS aperture, respectively. The response was normalized by the maximum power received for an open aperture without the FSS present. Fluctuations in the received S_{21} resulting from rapid variations in the radio channel environment (small scale fading) were removed by taking a running average over adjacent frequency points. The FSS structures presented in this paper are designed to block signals around 13 GHz to a depth of greater than −20 dB which is taken as the limit of acceptable performance which would be suitable for real-life applications, corresponding to 1% signal transmission through structure.[6]

The design of the inkjet printed RFID antenna is shown in Figure S7c. The antenna has a total size of 65 × 20 mm^2 including a port area, which is described in detail in our previous study.[7] The RFID integrated circuit chip used on all the tag designs was an NXP RFID ASIC (Application Specific Integrated Circuit) mounted on copper straps for contact with the RFID metal antenna. The NXP chip had a high frequency input impedance consisting of a resistive part, 15 Ohms, and a capacitive component equal to 128 Ohms at the RFID frequency. The RFID integrated circuit was connected to the metal antenna by direct ohmic contact and mechanically attached to the antenna by adhesive tape. The ohmic contact was achieved by applying point pressure to the copper straps and the underlying printed conductor. Tag read distance was measured using a Voyantic Tagformance lite RFID measurement system. After calibrating the system at 35 cm the RFID tag was transferred to the volunteers arm and the read range was extrapolated by measurement at the global RFID UHF frequency bands within permitted transmission power levels.

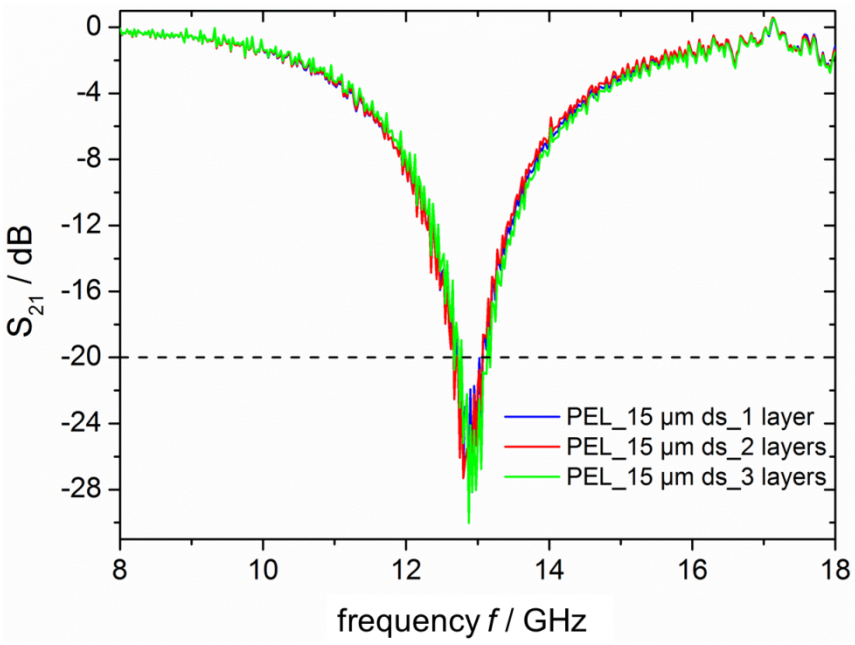

Figure S8 Transmission response (S_{21}) of single (blue), double (red) and triple (green) layer FSS inkjet printed with ink A on PEL paper upon thermally sintering (150 °C for 30 minutes).

Table S1 Summary of Inkjet printed FSS arrays, sintering conditions and resulting transmission response

Ink	Substrate	ds / µm	Layers	Sintering	S_{21} / dB	Ref
-	Copper coated polyester	n/a	1	n/a	< -30	[6]
Cabot CCI-300	PEN	10	1	thermal	-25	[8]
A	Tattoo paper	20	1	thermal	-23	-
A	Tattoo paper	20	1	plasma	<<<	-
A	Tattoo paper	20	1	photonic	-11	-
A	PEL paper	20	1	thermal	-17	-
A	PEL paper	15	1	thermal	-24	-
A	PEL paper	15	2	thermal	-25	-
A	PEL paper	15	3	thermal	-27	-
A	PEL paper	15	1	plasma	-23	-
A	PEL paper	15	1	photonic	-21	-
B	PEL paper	15	1	thermal	-11	-
B	PEL paper	20	1	plasma	-23	-

References

1 T. Öhlund, J. Örtegren, S. Forsberg, H.-E. Nilsson, *Appl. Surf. Sci.* 2012, *259*, 731-739.

2 H. Andersson, A. Manuilskiy, C. Lidenmark, J. Gao, T. Öhlund, S. Forsberg, J. Örtegren, W. Schmidt, H. E. Nilsson, *Nanotechnology* 2013, *24*, 455203.

3 M. Frenkel, in *The Chemistry of Inkjet Inks* (Ed.: S. Magdassi), World Scientific Publishing Co. Pte. Ltd., Singapore, 2010, pp. 73-97.

4 S. Kim, B. Cook, T. R. Le, J. Cooper, H. Lee, V. Lakafosis, R. Vyas, R. Moro, M. Bozzi, A. Georgiadis, A. Collado, M. M. Tentzeris, *IET Microw. Antennas Propag.* 2013, *7*, 858-868.

5 www.printedelectronics.co.uk/Information%20Sheet%20for%20PEL%20Nano%20P60.pdf

6 B. M. Turki, E. A. Parker, J. C. Batchelor, M. A. Ziai, V. Sanchez-Romaguera, S. G. Yeates, *Electron. Lett.* 2013, *49*, 1054-1055.

7 V. Sanchez-Romaguera, M. A. Ziai, D. Oyeka, S. Barbosa, J. S. R. Wheeler, J. C. Batchelor, E. A. Parker, S. G. Yeates, *J. Mater. Chem. C* 2013, *1*, 6395-6402.

8 J. C. Batchelor, E. A. Parker, J. A. Miller, V. Sanchez-Romaguera, S. G. Yeates, *Electron. Lett.* 2009, *45*, 7-8.

Graphical abstract: